

NUMERICAL STUDY OF MHD MIXED CONVECTION OF NANOFUID FLOW IN A DOUBLE LID CONVERGENT CAVITY

Bouchmel MLIKI^{1*}, Mokhtar FERHI^{2}, Mohamed Ammar ABBASSI^{3***}**

^{*}Research Lab, Technology Energy and Innovative Materials, Faculty of Sciences, University of Gafsa, Tunisia

^{**}CORIA, Normandie Université, INSA de Rouen, Technopôle du Madrillet, BP 8, Saint-Etienne-du-Rouvray 76801, France

^{***}Research Lab, Modeling, Optimization and Augmented Engineering, ISLAIB, University of Jendouba, Béja 9000, Tunisia

bouchmel.mliki@insa-rouen.fr, mokhtar.ferhi@gmail.com, abbassima@gmail.com

received 19 October 2024, revised 18 March 2025, accepted 24 March 2025

Abstract: This article presents a numerical analysis of mixed convection of a magnetic nanofluid in a double-lid driven convergent cavity. The Lattice Boltzmann Method (LBM) was used to solve the discretized system. The numerical results are illustrated through the flow, temperature, and local entropy generation fields. The study highlights the impact of several parameters, such as the Reynolds number (Re) (ranging from 1 to 100) for a Richardson number (Ri= 20), the Hartmann number (Ha) (ranging from 0 to 80), and the solid volume fraction (ϕ) (ranging from 0 to 0.04). The results show that both the total entropy generation and the average Nusselt number increases with the Reynolds number but decrease with increasing Hartmann number. Moreover, the numerical results show a significant increase in both the average Nusselt number and the total entropy generation with increasing nanoparticle volume fraction and Rayleigh number. Conversely, the Hartmann number exhibits an opposing effect, reducing both heat transfer and total entropy generation, with reductions of 30.18% and 32.15%, respectively, when Ha increases from 0 to 80. The findings of this study have significant applications in optimizing thermal management systems, such as cooling of electronic devices, energy-efficient HVAC systems, and industrial processes involving heat transfer enhancement.

Key words: mixed convection, entropy generation, nanofluid, magnetic field, LBM, convergent cavity

1. INTRODUCTION

In recent years, the mixed convection of magnetic nanofluids in various geometries has garnered increasing attention. Several studies have highlighted the diverse applications of this innovative class of nanofluids, including the works of Nandy and Yanuar [1], Soheli et al. [2], and Heris et al. [3]. Ahmed et al. [4] investigated the mixed convection of micropolar nanoliquids in a double lid-driven cavity. They reported an increase in the Nusselt number (Num) as the volume fraction (ϕ) increases, while it decreases as the length of the heat source increases.

Teamah et al. [5] investigated mixed convection in a square cavity filled with nanofluids. They observed that the mean Nusselt number (Num) increases with Reynolds (Re) and Rayleigh (Ra) numbers, but decreases as the volume fraction (ϕ) increases. In another innovative study, Garoosi et al. [6] numerically examined the mixed convection of nanoliquids. The effects of Re and Ra on heat transfer, fluid movement, and entropy generation in a nanoliquid-filled square cavity were studied by Mirmasoumi and Behzadmehr [7]. They found that Num increases with Re, Ra, and ϕ . Raisi et al. [8] studied the heat transfer by mixed convection of a Cu-water nanofluid in a vertical parallel plate channel. They found that an increase in the solid volume fraction leads to an enhancement in the heat transfer rate, particularly at low Richardson numbers. A numerical simulation of mixed convection in

inclined horizontal tubes with a uniform heat flux, using a nanofluid, was conducted by Akbari et al. [9]. The results showed that the Al₂O₃ concentration had no significant effect on the hydrodynamic parameters, and the heat transfer coefficient was maximal when the inclination angle was 45°.

In the presence of magnetic field effects, a numerical study on mixed convection in different geometries was conducted by Ali et al. [10, 11]. They suggest that the heat transfer rate depends on various physical parameters and geometric configurations. Furthermore, the heat transfer rate decreases with an increase in the magnetic field intensity. In another study, Kefayati [12] conducted a numerical examination of magnetic mixed convection. The analysis indicates that heat transfer decreases as the Hartmann number (Ha) increases. Akram et al. [13] studied MHD mixed convection in a chamfered square enclosure filled with water, analyzing the impact of magnetic field orientation on flow and heat transfer. Their results showed that both the intensity of the magnetic field and the inclination angle significantly influence heat transfer, with Nusselt numbers generally decreasing as the Hartmann number increases. Maya et al. [14] examined a lid-driven cavity with a rectangular heat source under the influence of a magnetic field, highlighting the importance of the Hartmann number in altering flow patterns and heat transfer rates.

Additionally, Mliki et al. [15, 16] studied mixed convection under the influence of the Lorentz force. They observed that in the presence of a magnetic field, the average Nusselt number along

the hot wall shows a significant dependence on several parameters. Specifically, this number increases with the Reynolds number (Re), which is generally associated with higher fluid velocity and flow intensity. On the other hand, the Nusselt number decreases with an increase in the Hartmann number (Ha). These results underscore the complex effect of the magnetic field on the mixed convection process and highlight the need to consider the interaction between these different parameters for more accurate modeling of thermal phenomena in conducting fluids. Also, Mliki et al. [17, 19] used LBM to examine the effect of nanoparticles Brownian motion on fluid movement in different geometries. Prosenjit et al. [20] used a commercial finite element solver "COMSOL Multiphysics 6.0 to examine the MHD mixed convection in a semicircular cavity with hybrid nanofluids. They found that the heat transfer increases with an increase in Ri but decreases with the rise of the Hartmann number (Ha). In another innovative study, Falah et al. [21] investigated the mixed convection phenomenon of a hybrid nanofluid flowing within a horizontally oriented channel, featuring a triangular cavity attached to the lower channel wall. They found that the average Nusselt number increases with higher Reynolds number, angular rotation speed, cylinder position, and Richardson number.

Mliki et al. [22] investigated the influence of a horizontal periodic magnetic field within a double-lid U-shaped enclosure. By comparing scenarios that included and excluded the effect of Brownian motion, they demonstrated that Brownian motion significantly enhances heat transfer under all defined conditions. In a related context, Ighris et al. [23, 24] explored the application of the Lattice Boltzmann Method (LBM) to model natural convection in hybrid nanofluids. Their work emphasized the advantages of this approach, particularly in terms of numerical stability and accuracy. Additionally, Hadoui et al. [30] studied natural double-diffusive convection in a square cavity filled with an Al_2O_3 -water-based nanofluid. Their findings revealed that the heat transfer rate increased with the nanoparticle volume fraction, while the mass transfer rate decreased. Recently, Thilagavathi et al. [25] conducted a study on heat transfer enhancement in a magnetic ternary hybrid nanofluid within a hexagonal cavity containing a square obstacle. The findings of this research demonstrate that the appropriate incorporation of nanoparticles significantly enhances the heat transfer properties of base fluids.

In recent years, magnetohydrodynamic (MHD) mixed convection of nanofluids in porous systems has attracted considerable attention due to its industrial and energy-related applications. For instance, Mandal et al. [26] investigated the MHD mixed convection of a hybrid nanofluid in a W-shaped porous system, emphasizing the influence of geometry and nanofluid properties on thermal and hydrodynamic transfer processes. Their findings demonstrated that thermal energy transfer significantly depends on the length of the heating and cooling surfaces, the fluid volume within the cavity, and the amplitude of the bottom undulation height in the W-shaped cavity. Additionally, Mandal et al. [27] examined the role of surface undulations during mixed bioconvective flow of a nanofluid in the presence of oxytactic bacteria and magnetic fields. Their study revealed that the complex interactions between magnetic forces, bioconvection, and the properties of the porous medium play a critical role in enhancing heat and mass transfer. In addition, Alomari et al. [28] performed a numerical analysis to examine the effect of a porous block on MHD mixed convection in a split lid-driven cavity containing a nanofluid. Their study demonstrated the significant impact of the porous block on thermal and hydrodynamic performance, particularly in complex configurations

such as split lid-driven cavities.

This study distinguishes itself through its innovative numerical analysis of mixed convection in a nanofluid (CuO /water) within a double-lid driven convergent cavity featuring discrete heating, under the influence of a horizontal magnetic field. Unlike previous studies, this research simultaneously investigates the combined effects of convergent cavity geometry, discrete heating, and a horizontal magnetic field on the thermal and dynamic characteristics of the flow.

2. PROBLEM DEFINITION

We consider the magnetic nanofluid mixed convection in a heated thermal convergent cavity. The configuration of the physical model is shown in Fig. 1. Two heat sources are situated at the left wall at constant temperature. The aspect ratio of the enclosure is defined as $AR = L/l = 0.3$. As visible from the graphical view, the superior and bottom walls of the cavity are cold and moving with a constant velocity (\vec{u}_0). The effect of periodic magnetic field (\vec{B}) is depicted in this figure. The thermal convergent is filled with CuO -Water Nanofluid (Tab. 1).

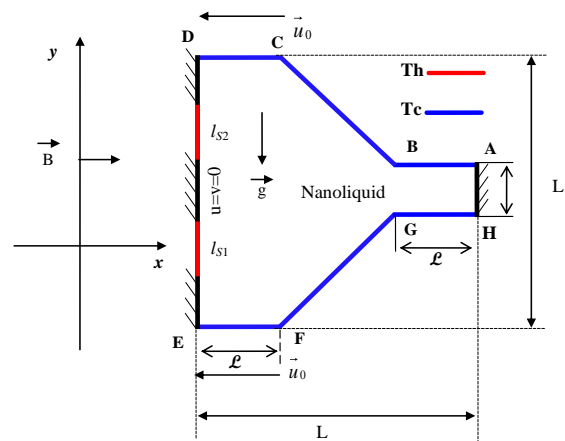


Fig. 1. Geometry of the problem

Tab. 1. Thermophysical properties of fluid and nanoparticles

Physical Properties	Fluid phase (H ₂ O)	Nanoparticle (CuO)
C_p (J/kg.K)	4179	385
ρ (kg/m ³)	997.1	8933
k (W/m.K)	0.631	401
$\beta \times 10^{-5}$ (1/K)	21	1.67
σ (Ω/m)-1	0.05	$5.69 \cdot 10^{-7}$

3. MATHEMATICAL FORMULATION

To investigate the mixed convection flow, certain assumptions are made to simplify the analysis.

3.1. Key Assumptions in the Study

Steady-State Flow: The study assumes that the flow is steady, meaning that the fluid properties (velocity, pressure, temperature, etc.) do not change with time.

Incompressible Flow: The fluid is assumed to be incompressible, implying that the density remains constant throughout the flow field. This assumption is valid for liquids and for gases at low Mach numbers (typically < 0.3).

Laminar Flow: The flow is assumed to be laminar, meaning that the fluid moves in smooth layers or streams without significant mixing. This assumption is reasonable for flows with low Reynolds numbers.

Negligible viscous dissipation: The study assumes that the energy generated by viscous dissipation is negligible. This means that the heat produced by internal friction within the fluid is insignificant compared to the other energy terms in the system.

Negligible Heat Generation: The study assumes that there is no significant heat generation within the fluid, either from chemical reactions, electrical heating, or other sources. This simplifies the energy equation by removing the heat generation term.

Constant Fluid Properties: The fluid properties such as viscosity, thermal conductivity, and specific heat are assumed to be constant. This assumption is valid for small temperature variations within the flow.

No Radiation Heat Transfer: The study assumes that heat transfer due to radiation is negligible compared to conduction and convection. This is reasonable for many engineering applications where temperatures are not extremely high.

3.2. Governing equations

By applying the Boussinesq approximation, the governing equations for this investigation are as follows [29]:

$$\frac{\partial u}{\partial x} + \frac{\partial v}{\partial y} = 0 \tag{1}$$

$$\rho_{nf} \left(u \frac{\partial u}{\partial x} + v \frac{\partial u}{\partial y} \right) = -\frac{\partial p}{\partial x} + \mu_{nf} \left(\frac{\partial^2 u}{\partial x^2} + \frac{\partial^2 u}{\partial y^2} \right) + F_x + f_{Lx} \tag{2}$$

$$\rho_{nf} \left(u \frac{\partial v}{\partial x} + v \frac{\partial v}{\partial y} \right) = -\frac{\partial p}{\partial y} + \mu_{nf} \left(\frac{\partial^2 v}{\partial x^2} + \frac{\partial^2 v}{\partial y^2} \right) + F_y + f_{Ly} \tag{3}$$

$$u \frac{\partial T}{\partial x} + v \frac{\partial T}{\partial y} = \alpha_{nf} \left(\frac{\partial^2 T}{\partial x^2} + \frac{\partial^2 T}{\partial y^2} \right) \tag{4}$$

For this problem, the fluid flow is subjected to gravitational force:

$$F_x = 0, \quad F_y = (\rho\beta)_{nf} g_y (T - T_c) \tag{5}$$

In addition to the gravitational force, the flow of the nanohybrid is subjected to the volumetric Laplace force:

$$f_{Lx} = 0, \quad f_{Ly} = -B^2 \cdot \sigma_{nf} v \tag{6}$$

To calculate this volumetric Laplace force, it is more appropriate to use the dimensionless Hartmann number, defined by:

$$Ha = LB \sqrt{\frac{\sigma_{nf}}{\mu_{nf}}} \tag{7}$$

This number is used in fluid dynamics, particularly in the study of conducting fluids in the presence of a magnetic field. It characterizes the influence of magnetic forces in relation to viscous forces within a fluid.

Where σ_{nf} is the electrical conductivity, B is the magnetic field intensity, L is the characteristic length of the cavity, and μ_{nf} is the dynamic viscosity of the nanofluid.

For Magneto-Hydro-Dynamic (MHD) nanofluid mixed con-

vection flow, the expression for local entropy generation, S_{gen} , can be formulated as follows [30]:

$$S_{gen} = \frac{k_{nf}}{T_0^2} \left[\left(\frac{\partial T}{\partial x} \right)^2 + \left(\frac{\partial T}{\partial y} \right)^2 \right] + \frac{\mu_{nf}}{T_0} \left[2 \left(\frac{\partial u}{\partial x} \right)^2 + 2 \left(\frac{\partial v}{\partial y} \right)^2 + \left(\frac{\partial u}{\partial y} + \frac{\partial v}{\partial x} \right)^2 \right] + \frac{\sigma_{nf} B^2}{T_0} v^2 = S_{gen,h} + S_{gen,v} + S_{gen,m} \tag{8}$$

The effective density, heat capacitance, thermal expansion coefficient, thermal diffusivity, and electrical conductivity of the nanofluid are defined as follows [31]:

$$\rho_{nf} = (1 - \phi) \rho_f + \phi \rho_p \tag{9}$$

$$(\rho C_p)_{nf} = (1 - \phi) (\rho C_p)_f + \phi (\rho C_p)_p \tag{10}$$

$$(\rho\beta)_{nf} = (1 - \phi) (\rho\beta)_f + \phi (\rho\beta)_p \tag{11}$$

$$\alpha_{nf} = \frac{k_{nf}}{(\rho C_p)_{nf}} \tag{12}$$

$$\frac{\sigma_{nf}}{\sigma_f} = 1 + \frac{3 \left(\frac{\sigma_s}{\sigma_f} - 1 \right) \phi}{\left(\frac{\sigma_s}{\sigma_f} + 2 \right) - \left(\frac{\sigma_s}{\sigma_f} - 1 \right) \phi} \tag{13}$$

The thermal conductivity of the nanofluid is determined using the following equation [32]:

$$k_{static} = k_f \frac{k_p + 2k_f - 2\phi(k_f - k_p)}{k_p + 2k_f + \phi(k_f - k_p)} \tag{14}$$

The effective dynamic viscosity of the nanofluid is determined using the Brinkman model [33]:

$$\mu_{static} = \frac{\mu_f}{(1 - \phi)^{2.5}} \tag{15}$$

A numerical investigation of mixed convection was carried out using the following dimensionless variables:

$$\begin{aligned} X = \frac{x}{L}, \quad Y = \frac{y}{L}, \quad U = \frac{u}{U_0}, \quad V = \frac{v}{U_0}, \quad \theta = \frac{T - T_c}{T_h - T_c}, \\ Pr = \frac{\nu_{nf}}{\alpha_{nf}}, \quad P = \frac{p}{\rho_{nf} U_0^2}, \quad Gr = \frac{g\beta(T - T_c)L^3}{\nu_{nf}^2}, \\ Re = \frac{U_0 L}{\nu_{nf}}, \quad Ri = \frac{Gr}{Re^2}, \quad Ha = LB \sqrt{\frac{\sigma_{nf}}{\mu_{nf}}}, \quad S_T = \\ S \frac{T_0^2 L^2}{k_{nf} (T_h - T_c)^2} \end{aligned} \tag{16}$$

The Reynolds number (Re) is one of the most important dimensionless parameters in fluid mechanics. It is used to characterize the flow regime of a fluid, whether it is laminar, transitional, or turbulent. It is defined as the ratio of inertial forces to viscous forces in a fluid flow.

By introducing the dimensionless variables mentioned above, the governing equations (1-4) are transformed into their non-dimensional forms, which can be expressed as follows:

$$\frac{\partial U}{\partial X} + \frac{\partial V}{\partial Y} = 0 \tag{17}$$

$$U \frac{\partial U}{\partial X} + V \frac{\partial U}{\partial Y} = -\frac{\partial P}{\partial X} + \frac{1}{Re} \frac{\rho_f}{\rho_{nf}} \frac{1}{(1 - \phi)^{2.5}} \left(\frac{\partial^2 U}{\partial X^2} + \frac{\partial^2 U}{\partial Y^2} \right) \tag{18}$$

$$U \frac{\partial V}{\partial X} + V \frac{\partial V}{\partial Y} = -\frac{\partial P}{\partial Y} + \frac{1}{Re} \frac{\rho_f}{\rho_{nf}} \frac{1}{(1 - \phi)^{2.5}} \left(\frac{\partial^2 V}{\partial X^2} + \frac{\partial^2 V}{\partial Y^2} \right) \tag{19}$$

$$+ Ri \frac{\rho_f}{\rho_{nf}} \left(1 - \phi + \frac{(\rho\beta)_p}{(\rho\beta)_f} \right) \theta - \frac{\rho_f}{\rho_{nf}} \frac{\sigma_{nf}}{\sigma_f} \frac{Ha^2}{Re} V$$

$$U \frac{\partial \theta}{\partial X} + V \frac{\partial \theta}{\partial Y} = \frac{\alpha_{nf}}{\alpha_f} \frac{1}{Re Pr} \left(\frac{\partial^2 \theta}{\partial X^2} + \frac{\partial^2 \theta}{\partial Y^2} \right) \quad (20)$$

Dimensionless entropy generation S_{gen} can be obtained as:

$$S_T = \frac{k_{nf}}{k_f} \left[\left(\frac{\partial \theta}{\partial X} \right)^2 + \left(\frac{\partial \theta}{\partial Y} \right)^2 \right] + \chi \frac{\mu_{nf}}{\mu_f} \left[2 \left(\frac{\partial U}{\partial X} \right)^2 + 2 \left(\frac{\partial V}{\partial Y} \right)^2 + \left(\frac{\partial U}{\partial Y} + \frac{\partial V}{\partial X} \right)^2 \right] - \chi_{nf} Ha^2 \frac{\sigma_{nf}}{\sigma_f} V^2 \quad (21)$$

where χ is the irreversibility factor. It is defined by:

$$\chi_{nf} = \frac{\mu_f T_0}{k_f} \left(\frac{U_0}{T_h - T_c} \right)^2 \quad (22)$$

The average entropy generation is calculated by:

$$S_{avr} = \frac{1}{V} \int_V S_T dV \quad (23)$$

where V is the total volume of the physical domain.

The local and average Nusselt numbers along the two heat sources (IS1, IS2) can be calculated using the following expressions:

$$Nu = - \frac{k_{nf}}{k_f} \left(\frac{\partial \theta}{\partial X} \right) \Big|_{X=0} \quad (24)$$

$$\overline{Nu}_{IS_1} = \int_{0.2}^{0.4} Nu \, dY, \quad (25)$$

$$Nu_{IS_2} = \int_{0.6}^{0.8} Nu \, dY$$

4. NUMERICAL METHOD AND VALIDATION

The given equations have been numerically solved using the lattice Boltzmann method (LBM), as detailed in Mliki et al. [31]. This approach was based on Ludwig Boltzmann's kinetic theory of gases. Employing the Bhatnagar-Gross-Krook approximation, the lattice Boltzmann method involves two distribution functions, denoted as g and f , representing the temperature and the flow field, respectively, Eqs. (26) and (27):

$$f_i(\mathbf{x} + \mathbf{c}_i \Delta t, t + \Delta t) = f_i(\mathbf{x}, t) - \frac{1}{\tau_v} \left(f_i(\mathbf{x}, t) - f_i^{eq}(\mathbf{x}, t) \right) + \Delta t \mathbf{c}_i F_i \quad (26)$$

$$g_i(\mathbf{x} + \mathbf{c}_i \Delta t, t + \Delta t) = g_i(\mathbf{x}, t) - \frac{1}{\tau_\alpha} \left(g_i(\mathbf{x}, t) - g_i^{eq}(\mathbf{x}, t) \right) \quad (27)$$

Here, Δt represents the lattice time, and τ_v and τ_α denote the lattice relaxation times for the flow and temperature fields, respectively.

Two local equilibrium distribution functions for the temperature and flow fields g_i^{eq} and f_i^{eq} are calculated with Eqs. (28) and (29):

$$f_i^{eq} = \omega_i \rho \left[1 + \frac{3(\mathbf{c}_i \cdot \mathbf{u})}{c^2} + \frac{9(\mathbf{c}_i \cdot \mathbf{u})^2}{2c^4} - \frac{3u^2}{2c^2} \right] \quad (28)$$

$$g_i^{eq} = \omega'_i T \left[1 + 3 \frac{\mathbf{c}_i \cdot \mathbf{u}}{c^2} \right] \quad (29)$$

The variables u and \mathbf{p} represent the macroscopic velocity and

density, respectively. The lattice speed c is defined as $c = \Delta x / \Delta t$, where Δx is the lattice spacing and Δt is the lattice time step, both of which are set to unity. Furthermore, ω_i denotes the weighting factor for the flow field, while ω'_i represents the weighting factor for the temperature field. The D2Q9 model is used for the flow field, while the D2Q4 model is applied to the temperature field.

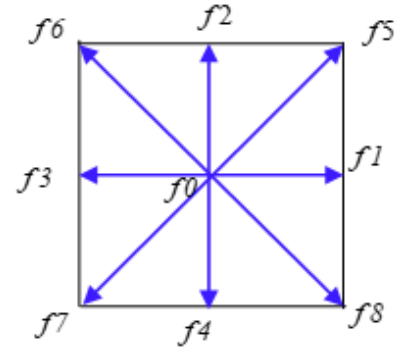


Fig. 2. Direction of streaming velocities, D₂Q₉

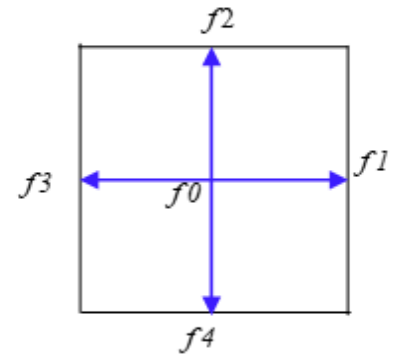


Fig. 3. Direction of streaming velocities, D₂Q₄

Consequently, the weighting factors and discrete particle velocity vectors differ between these two models and are calculated using Eqs. (30-33) as follows:

For D₂Q₉:

$$\omega_0 = \frac{4}{9}, \omega_i = \frac{1}{9} \text{ for } i = 1,2,3,4 \text{ and } \omega_i = \frac{1}{36} \text{ for } i = 5,6,7,8 \quad (30)$$

The discrete velocities for the D₂Q₉ (Fig. 2) are defined as follows:

$$c_i = \begin{cases} 0 & i = 0 \\ (\cos[(i-1)\pi/2], \sin[(i-1)\pi/2])c & i = 1,2,3,4 \\ \sqrt{2}(\cos[(i-5)\pi/2 + \pi/4], \sin[(i-5)\pi/2 + \pi/4])c & i = 5,6,7,8 \end{cases} \quad (31)$$

For D₂Q₄:

The weighting factor for temperature in each direction is:

$$\omega'_i = \frac{1}{4} \quad (32)$$

The discrete velocities for the D₂Q₄ (Fig. 3) are defined as follows:

$$c_i = (\cos[(i-1)\pi/2], \sin[(i-1)\pi/2])c \quad i = 1,2,3,4 \quad (33)$$

The relationship between the kinematic viscosity ν and ther-

mal diffusivity α with the relaxation time is expressed by Eq. (34):

$$v = \left[\tau_v - \frac{1}{2} \right] c_s^2 \Delta t; \quad \alpha = \left[\tau_\alpha - \frac{1}{2} \right] c_s^2 \Delta t \quad (34)$$

Where c_s is the lattice speed of sound, equal to $c_s = c/\sqrt{3}$. In the simulation of natural convection, the external force term F_i is determined by Eq. (35):

$$F_i = \frac{\omega_i}{c_s^2} F \cdot c_i \quad (35)$$

With F_i is the total external body force.

The macroscopic quantities ρ , u , and T can be calculated by Eq. (36):

$$\rho = \sum_i f_i; \quad \rho u = \sum_i f_i c_i; \quad T = \sum_i g_i \quad (36)$$

5. SOLUTION METHOD

To ensure the applicability of the code in a nearly incompressible regime, the characteristic velocity must be significantly lower than the speed of sound in the fluid. Therefore, in the simulations, the Mach number is set to less than $Ma=0.3$. In this study, the Mach number is fixed at $Ma=0.1$ for all considered cases. Viscosity and thermal diffusivity are determined based on the definitions of the corresponding dimensionless parameters, while maintaining constant values for the Rayleigh number, Prandtl number, and Mach number.

$$v_f = NMac_s \sqrt{\frac{Pr}{Ra}} \quad (37)$$

With N indicating the total number of lattices positioned in the y -direction.

The stream function and vorticity are defined as:

$$\frac{\partial^2 \psi}{\partial x^2} + \frac{\partial^2 \psi}{\partial y^2} = -\left(\frac{\partial v}{\partial x} - \frac{\partial u}{\partial y} \right) = -\omega \quad (38)$$

where ω and ψ are vorticity and stream function, respectively.

6. MESH VERIFICATION AND VALIDATION

For the grid sensitivity analysis, Tab. 2 presents the results obtained using four different mesh sizes. The simulations revealed that the difference in results between the grid sizes of 100×100 and 150×150 was minimal. Based on these findings, the grid size of 100×100 was selected for the analysis.

Tab 2. Grid independence test for \overline{Nu}_m at $\phi=4.10^{-2}$; $Ha = 0$

Lattice size	Average Nusselt number \overline{Nu}_m	
	Re=1	Re=100
50x50	1.7632	7.3423
75x75	2.1482	8.8753
100x100	2.5483	9.6128
120x120	2.5502 (0.07%)	9.6412 (0.2%)

For data validation, the present results are compared with the numerical results from Lai and Yang [34] for the case of nanofluid natural convection in a square enclosure (Fig. 4).

Additionally, the temperature distribution along the axial mid-

line is compared between the present results and those obtained by Ghassemi et al. [35] for magnetic nanofluid mixed convection in a square enclosure (Fig. 5). Another validation test is performed for the case of mixed convection (Fig. 6), where the current numerical results are compared with the results from Talebi et al. [36]. Based on these comparisons, the developed code is demonstrated to be reliable for studying MHD mixed convection of a nanofluid in a double-lid driven thermally convergent cavity.

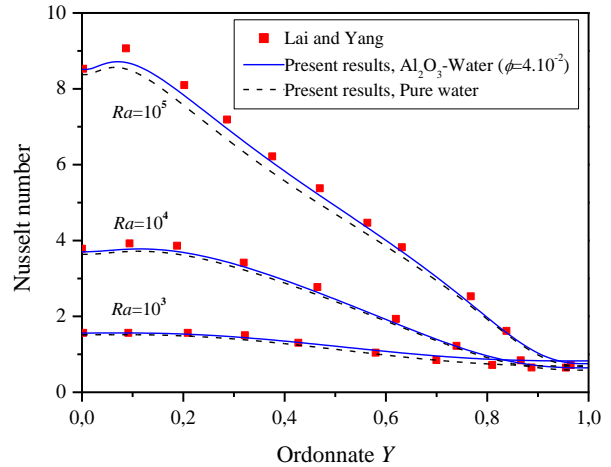


Fig. 4. Comparison of the local Nusselt number along the hot wall between the present results and numerical results by Lai and Yang [34]

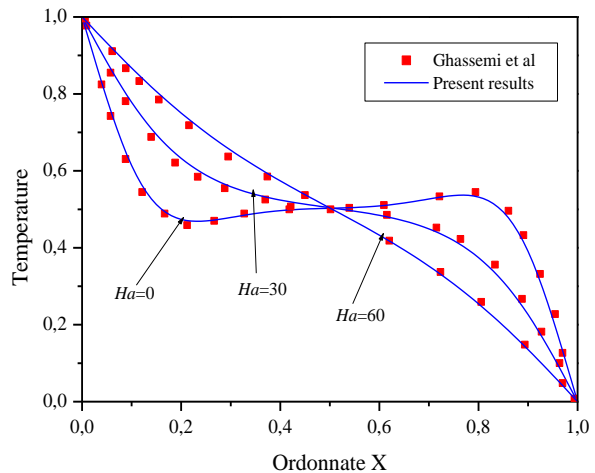
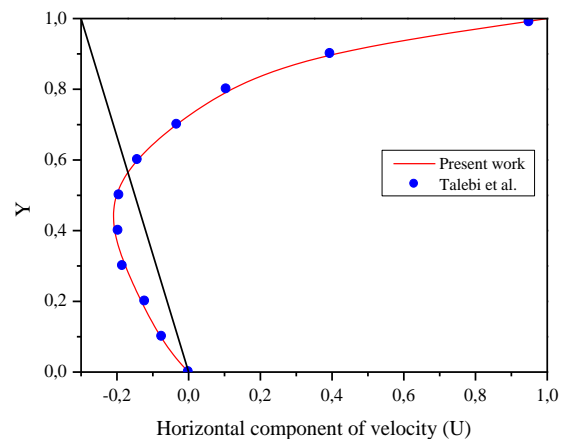
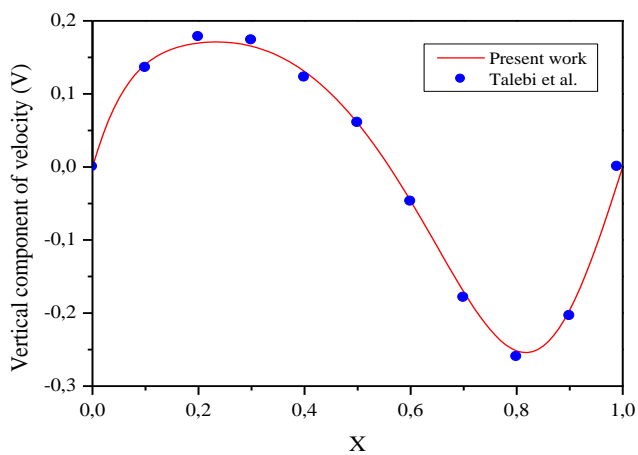


Fig. 5. Comparison of the temperature on axial midline between the present results and numerical results by Ghassemi et al. [35] ($\phi=3.10^{-2}$, $Ra=10^5$)



(a)



(b)
Fig. 6. a) Horizontal component of velocity b) vertical component of velocity with those of Talebi et al. [36]

7. RESULTS AND DISCUSSION

A numerical analysis of two-dimensional magnetohydrodynamic (MHD) mixed convection is conducted for a CuO–water nanofluid within a double lid-driven thermally convergent cavity. The study investigates the fluid flow and heat transfer characteristics under the influence of magnetic fields, focusing on the behavior of the nanofluid in this specific configuration.

7.1. Effects of Reynolds number

The main objective of this numerical study is to evaluate the effects of the Reynolds number (Re) on isotherms, local entropy generation, and streamlines inside the cavity saturated with CuO-water nanofluid, for $Ri = 20$, $\phi = 4.10^{-2}$, and $Ha = 0$. For $Re = 1$, the flow, local entropy generation, and temperature contours are nearly symmetric about the horizontal centerline ($Y = 0.5$) of the cavity and are concentrated along the two heated sources (IS1 and IS2) due to the enhanced fluid movement in these regions. In this case, the flow is characterized by the presence of two symmetric counterclockwise vortices, rotating in opposite directions with intensities ($|\psi|_{max} = 7.16 \times 10^{-2}$ and 6.91×10^{-2}), respectively (Fig. 7). As the Reynolds number increases, the influence of the moving walls (CD and EF) becomes increasingly significant, leading to substantial changes in the flow dynamics within the cavity. These walls, moving relative to the fluid, introduce a forced convection component that enhances fluid circulation in the surrounding regions. This effect is especially prominent in the lower part of the cavity, where the largest circulation cell develops.

In this figure, at low Reynolds numbers ($Re = 1$), heat transfer within the cavity is primarily dominated by conduction, with isotherms appearing nearly parallel to the isothermal walls. As the Reynolds number increases ($Re = 10, 50$, and 100), the cold nanofluid penetrates deeper into the corners (D and E), intensifying the temperature gradients around the discrete heat sources (IS1 and IS2). Additionally, enhanced circulation of the nanofluid is observed on the left side of the cavity (zone ABGH), resulting in a more efficient heat transfer process. The effect of increasing the Reynolds number on entropy generation is also illustrated in Fig.7. It is observed that an increase in the Reynolds number enhances fluid motion, resulting in a higher concentration of entropy genera-

tion contours near the discrete heat sources. This leads to the formation of active regions of entropy generation, which are particularly pronounced at higher Reynolds numbers ($Re = 10, 50$, and 100).

In summary, an increase in the Reynolds number significantly modifies the distribution and intensity of entropy generation within the cavity. These changes are primarily driven by the intensification of forced convection, which enhances temperature and velocity gradients, leading to the formation of active entropy generation zones near the heat sources and in regions of increased fluid circulation. These findings underscore the importance of accounting for the effects of the Reynolds number in the design and optimization of heat transfer systems that utilize nanofluids.

The effect of solid nanoparticle concentration on the Nusselt number (Num) along the discrete heat sources (IS1 and IS2) is illustrated in Fig.8. A detailed analysis of Equation (14) shows that increasing the concentration of solid nanoparticles in the nanofluid directly enhances its effective thermal conductivity. This enhancement is critical, as it improves heat transfer through the fluid, particularly in the regions near the heat sources where the heat transfer intensity is highest. As a result, the fluid becomes more effective in transferring heat, leading to an increase in the Nusselt number. In Fig.9, the total entropy generation (S_{gen}) exhibits a trend similar to that of the Nusselt number (Num). This correlation can be explained by the fact that the enhancement of heat transfer, driven by the increase in nanoparticle concentration, is accompanied with an increase in thermodynamic irreversibilities, as measured by entropy generation.

Figs 10 and 11 illustrate the temperature profile within the cavity at two specific positions: $x/L = 0.5$ and $y/L = 0.75$, for different Reynolds numbers (Re). These graphs provide a detailed analysis of how temperature evolves within the cavity as Re changes. It is clearly observed that the temperature in the ABGH region of the cavity increases with higher Re . This trend can be attributed to the increasing influence of mixed convection heat transfer, which becomes more dominant as Re rises. At low Reynolds numbers, heat transfer is mainly governed by thermal conduction, a slower and less efficient mechanism for heat transfer. However, as Re increases, mixed convection enhances heat transfer, leading to a more significant temperature rise in regions close to the heated walls of the cavity, particularly in the ABGH area. This behavior underscores the importance of fluid velocity and the convection regime in optimizing heat transfer within confined systems such as the one studied. These findings highlight the critical role of Reynolds number in controlling heat transfer dynamics and suggest that optimizing fluid flow conditions can significantly improve the efficiency and reliability of thermal management systems in practical applications.

7.2. Effects of Hartmann number

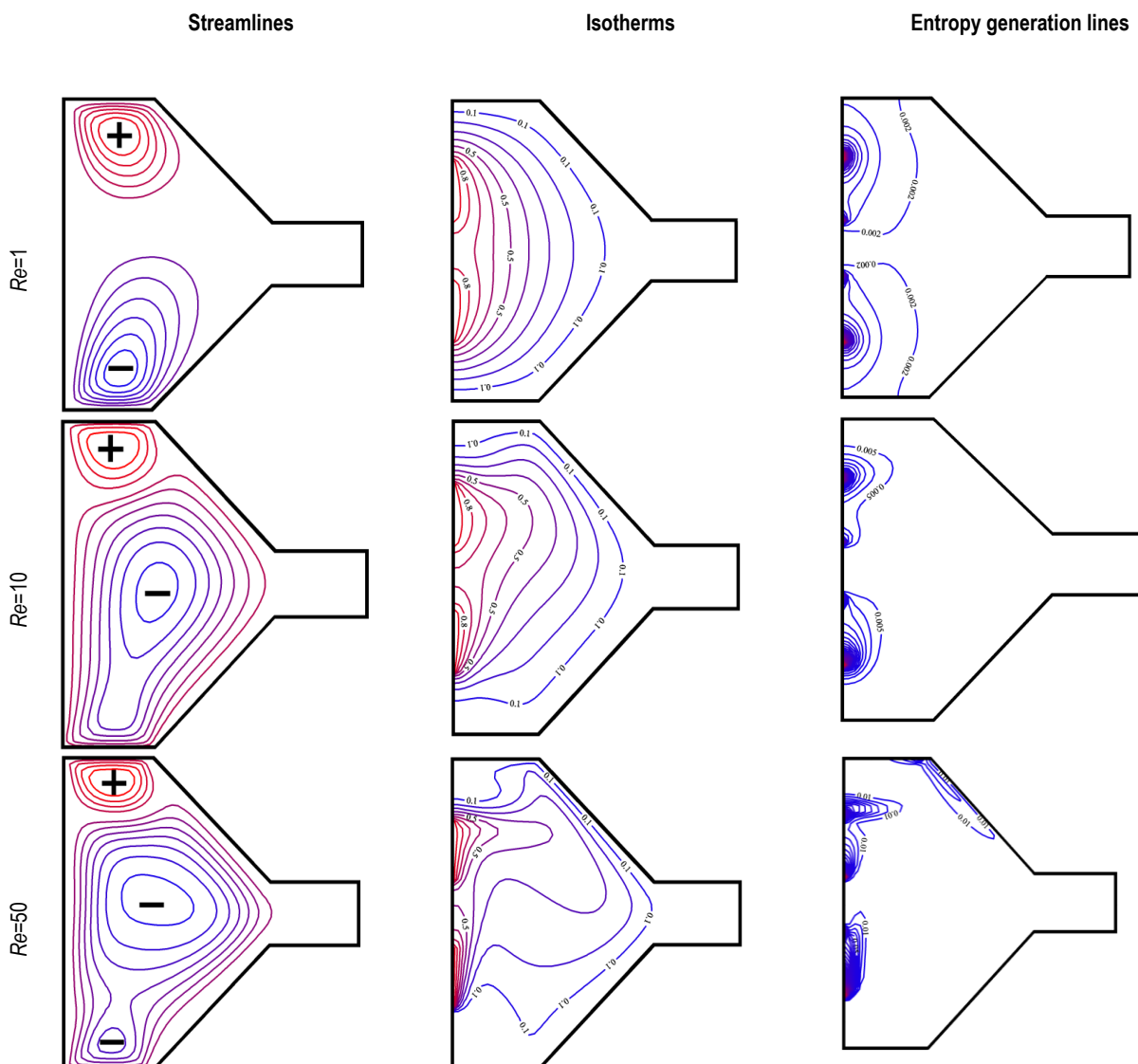
The effects of the Hartmann number (Ha) on the streamlines and entropy generation contours for $Re = 100$, $Ri = 20$, and $\phi = 4.10^{-2}$ are shown in Fig.12. The presence of a magnetic field leads to a significant reduction in mixed convection, resulting in an unfavorable impact on heat transfer. While buoyancy enhances heat transfer, the Lorentz force induced by the magnetic field counteracts this effect, reducing thermal transfer efficiency and minimizing entropy generation, making the process less favorable for optimizing heat transfer. As observed, an increase in the Hartmann number results in a reduction in flow intensity, with the

minimum value occurring at the highest Hartmann number. The maximum value of the stream function is 3.68×10^{-1} for $Ha = 0$, 2.94×10^{-1} for $Ha = 20$, and 1.5×10^{-1} for $Ha = 80$, which explains the stagnation of the stream function at $Ha = 80$. This flow stagnation at high Hartmann numbers has significant implications for heat transfer dynamics. Specifically, the reduction in mixed convection results in a greater dominance of thermal conduction. As a consequence, while entropy generation is reduced due to the decrease in irreversibilities associated with fluid motion, the overall heat transfer efficiency is diminished.

Fig. 13. illustrates the effect of the Lorentz force on the variation of the average Nusselt number and total entropy generation for different Hartmann numbers ($Ha = 0, 20, 40, 60$ and 80) at a solid particle concentration of $\phi = 0.04$. It can generally be observed that the average Nusselt number decreases as the Hartmann number (Ha) increases. This decrease is primarily attributed to the inhibitory effect of the Lorentz force, which opposes fluid motion and reduces the intensity of mixed convection. In the absence of a magnetic field ($Ha = 0$), the average Nusselt number reaches its maximum value, reflecting optimal mixed convection and efficient heat transfer. However, as Ha increases, the Lorentz force becomes more dominant, slowing

down the flow and thereby reducing the contribution of convection to heat transfer. Consequently, heat transfer becomes increasingly dominated by conduction, a less efficient mechanism compared to convection. The variation in entropy generation follows a trend similar to that of the Nusselt number. At low Hartmann numbers ($Ha = 0$), entropy generation is relatively high due to the irreversibilities associated with intense fluid motion and pronounced temperature gradients. However, as Ha increases, the reduction in flow intensity decreases these irreversibilities, leading to a gradual decline in entropy generation.

Figs. 14 and 15 show the temperature profile within the cavity at two specific positions: $x/L = 0.5$ and $y/L = 0.75$, for different Hartmann numbers (Ha). These graphs provide a detailed analysis of how the temperature evolves within the cavity as Ha changes. It is clearly observed that the temperature in the *ABGH* region of the cavity decreases as Ha increases. This trend can be attributed to the reduced influence of mixed convection heat transfer, which becomes less significant as Ha increases. At high Hartmann numbers, heat transfer is primarily governed by thermal conduction. This results in a more significant decrease in temperature in the *ABGH* region.



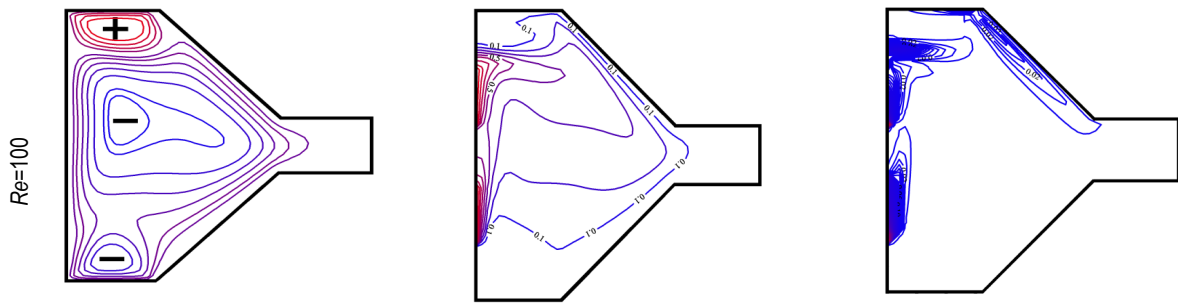


Fig.7. Streamlines, Isotherms and Entropy generation lines for different Re at $Ri=20$, $Ha=0$, and $\phi= 4 \cdot 10^{-2}$

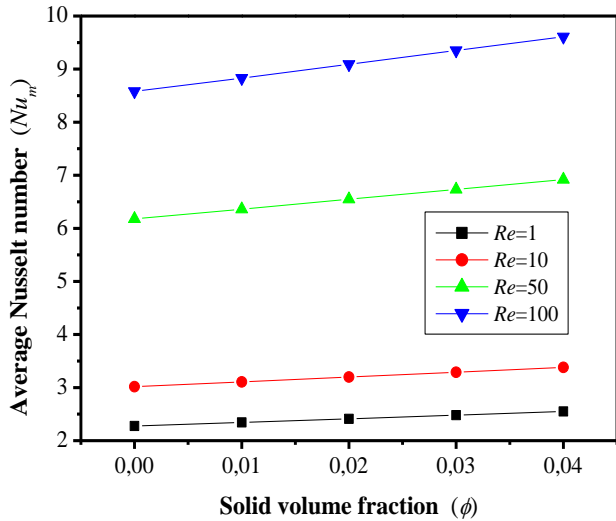


Fig.8. Average Nusselt number for different values of the Reynolds numbers and volumetric fraction of nanoparticles (ϕ) at $Ri=20$, $Re=100$ and $Ha=0$

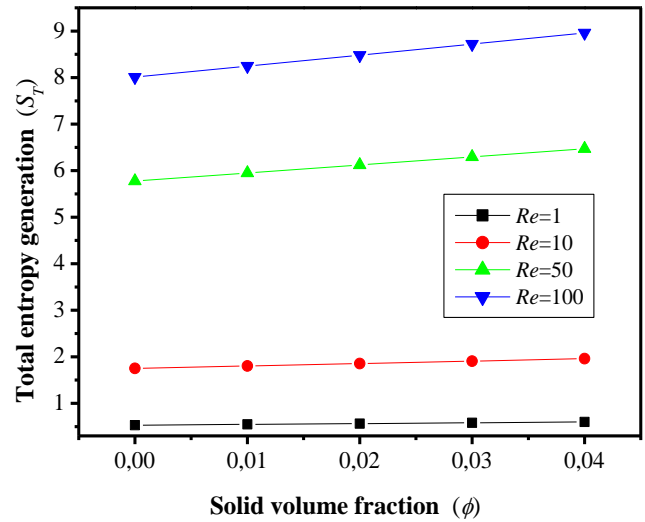


Fig.9. Total entropy generation for different values of the Reynolds numbers and volumetric fraction of nanoparticles (ϕ) at $Ri=20$, $Re=100$ and $Ha=0$

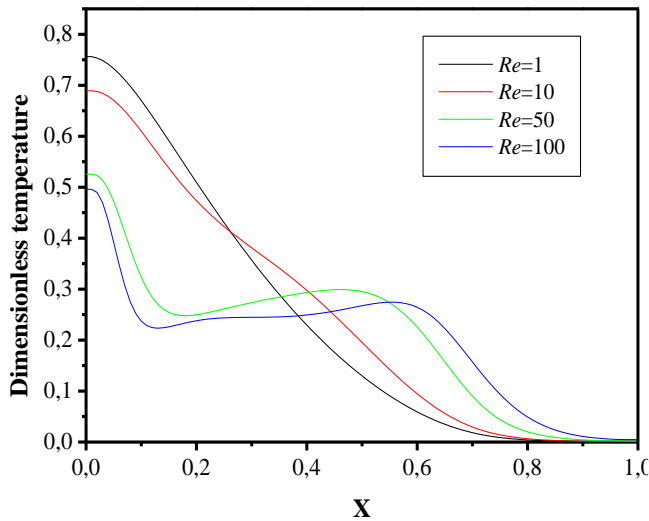


Fig.10. Profiles of the dimensionless temperature in the middle of the thermally convergent cavity $y/L = 0.5$ for different Reynolds numbers at $Ri=20$, $Ha=0$ and $\phi= 4 \cdot 10^{-2}$

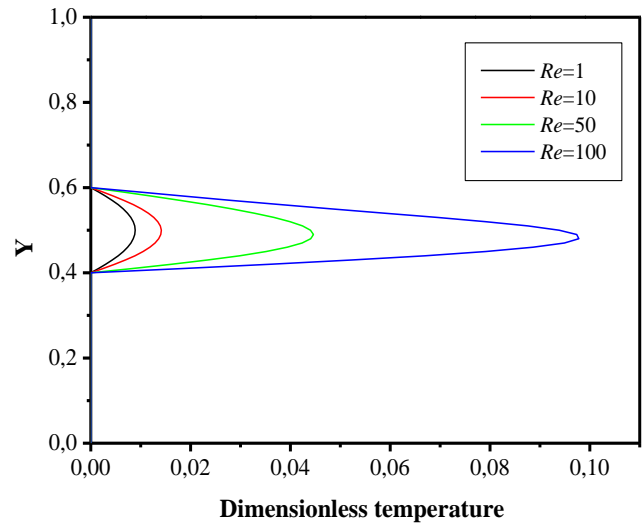


Fig.11. Profiles of the dimensionless temperature in the middle of the thermally convergent cavity $x/L = 0.75$ for different Reynolds numbers at $Ri=20$, $Ha=0$ and $\phi= 4 \cdot 10^{-2}$

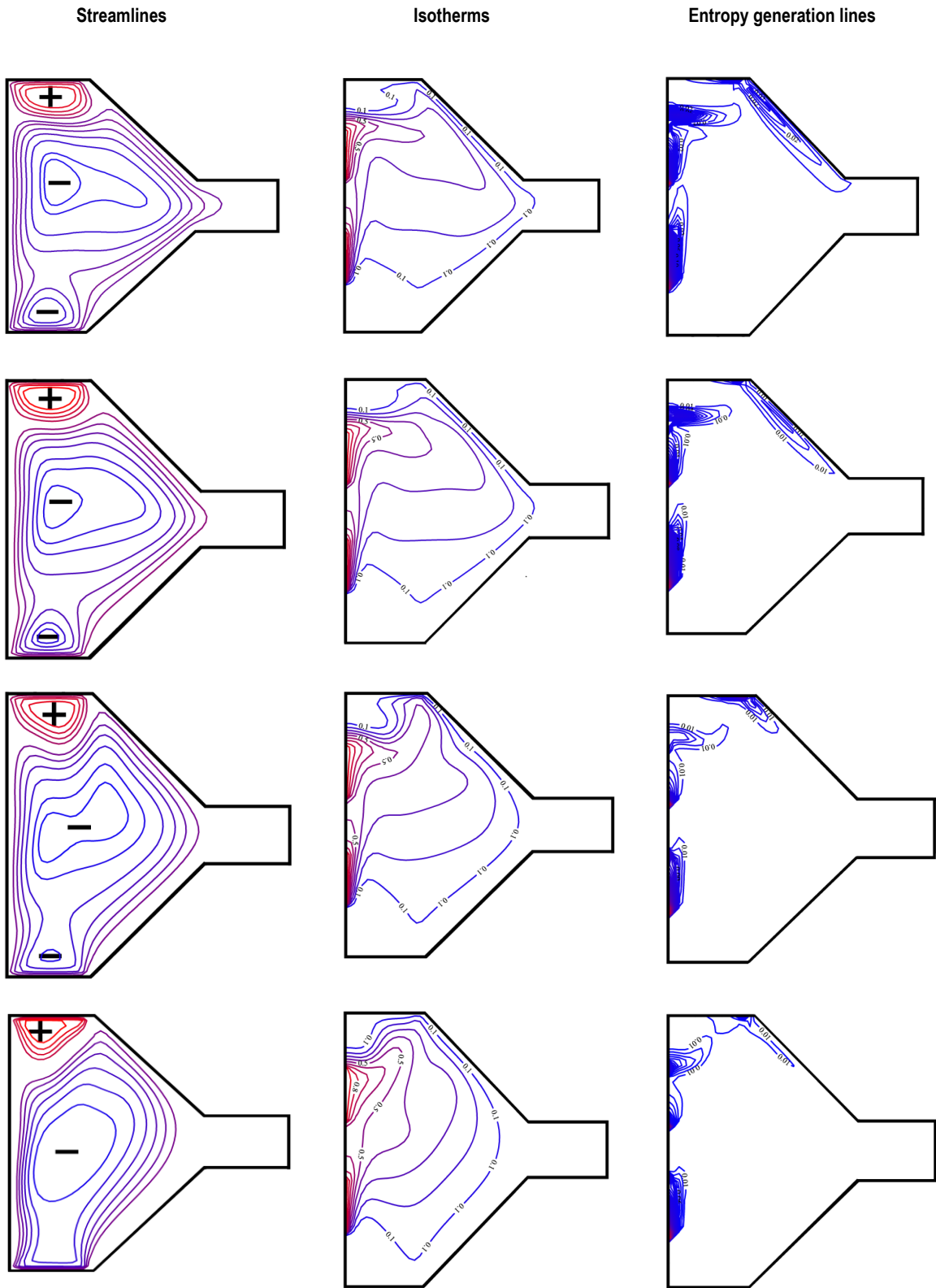


Fig. 12. Streamlines, Isotherms and Entropy generation lines for different Ha at Re =100, Ri=20 and $\phi= 4.10^{-2}$

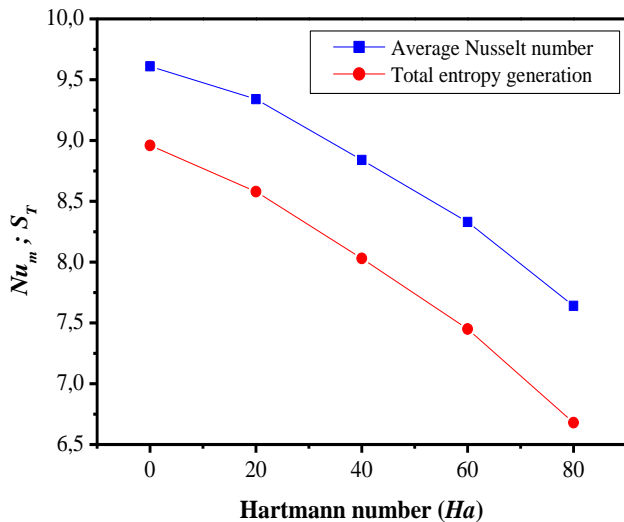


Fig. 13. Effect of Hartmann number on average Nusselt number and on total entropy generation for different Hartmann numbers at $Ri = 20$, $Re = 100$ and $\phi = 4.10^{-2}$

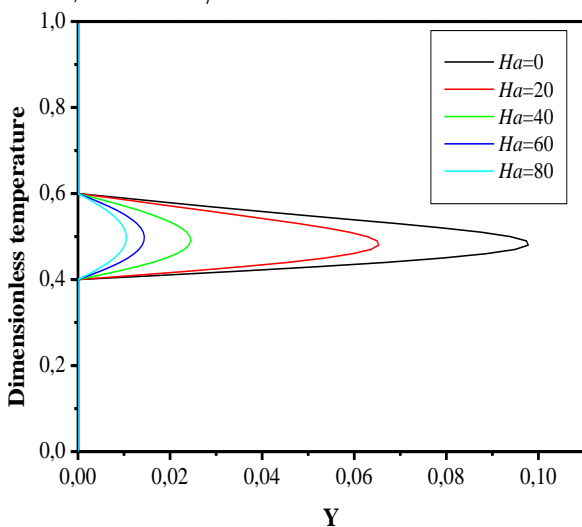


Fig. 14. Profiles of the dimensionless temperature in the middle of the thermally convergent cavity $x/L = 0.75$ for different Hartmann numbers at $Ri = 20$, $Re = 100$ and $\phi = 4.10^{-2}$

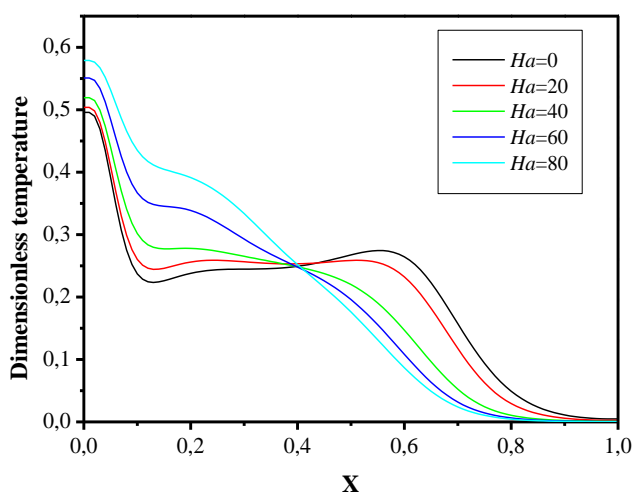


Fig. 15. Profiles of the dimensionless temperature in the middle of the thermally convergent cavity $y/L = 0.5$ for different Hartmann numbers at $Ri = 20$, $Re = 100$ and $\phi = 4.10^{-2}$

8. CONCLUSION

This study introduces an innovative approach to investigate mixed convection heat transfer by analyzing the influence of a magnetic field on heat transfer and flow characteristics in a convergent double-lid-driven cavity with discrete heating. The effects of the Reynolds number (Re), Hartmann number (Ha), and nanoparticle volume fraction (ϕ) on flow dynamics and heat transfer performance were systematically examined. The primary conclusions derived from the numerical results are as follows:

- For all considered values of Re and Ha , increasing the nanoparticle volume fraction leads to an increase in the average Nusselt number and total entropy generation.
- As the Reynolds number (Re) the values of the Nusselt number (Num) also increase.
- The maximum value of the stream function ($|\psi|_{max}$) is achieved at $Re = 100$.
- When a magnetic field is applied, the velocity of the nanofluid decreases, which in turn leads to a reduction in the maximum value of $|\psi|_{max}$.
- Both the Nusselt number (Num) and entropy generation are inversely related to the Hartmann number (Ha).
- The temperature in convergent cavity increases with an increase in Re , whereas the opposite effect is observed when Ha increases.
- The influence of Ha on Num and entropy generation is more pronounced at higher Reynolds numbers ($Re = 50$ and 100).

Based on the results presented in this article, it is recommended to use a combination of $Re = 100$, $Ha = 0$ (absence of a magnetic field), and $\phi = 0.04$ to maximize heat transfer. However, if entropy generation must be minimized, a compromise with $Ha = 80$ is suggested. This higher Hartmann number value will improve flow control and reduce entropy generation while maintaining acceptable heat transfer performance. This approach is particularly beneficial in applications where energy efficiency and loss minimization are top priorities.

REFERENCES

1. Nandy P, Iskandar F N. Application of nanofluid to a heat pipe liquid-block and the thermoelectric cooling of electronic equipment. *Exp Therm Fluid Sci.* 2011; 5:1274–1281.
2. Sohel MR, Saidur R, Mohd S M, Ijam A. Investigating the heat transfer performance and thermophysical properties of nanofluid in a circular micro-channel. *Int Commun Heat Mass Transf.* 2013; 42:75–81.
3. Heris SZ, Esfahany MN, Etemad SG. Experimental investigation of convective heat transfer of AL2O3/H2O nanofluid in circular tube. *Int J Heat Fluid Flow.* 2007; 28:203–10.
4. Ahmed S E, Mansour M A, Hussein, A K and Sivasankaran S. Mixed convection from a discrete heat source. *Engineering Science and Technology, an International Journal*, 2016; 19: 364-376.
5. Teamah MA, Sorour M M, El-Maghlany W M and Afifi A. Numerical simulation of double diffusive laminar mixed convection. *Alexandria Engineering Journal.* 2013; 52: 227-239.
6. Garoosi F, Rohani B, Rashidi MM. Two-phase mixture modeling of mixed convection of nanofluids in a square cavity. *Powder Technology.* (2015), 275: 304–321.
7. Mirmasoumi S, Behzadmehr A. Effect of nanoparticles mean diameter on mixed convection heat transfer of a nanofluid in a horizontal tube. *Int. J. Heat Fluid.* 2008; 29: 557–56.
8. Raisi A, Aminossadati S M and Ghasemi B. Magnetohydrodynamic mixed convection of a cu-water nanofluid in a vertical channel. *Journal of Heat Transfer.* 2013; 135.

9. Akbari M, Behzadmehr A and Shahraki F. Fully developed mixed convection in horizontal and inclined tubes with uniform heat flux using Nanofluid. *International Journal of Heat and Fluid Flow*. 2008; 29: 545-556.
10. Ali MM, Alim MA, Ahmed SS. Oriented magnetic field effect on mixed convective flow of nanofluid in a grooved channel with internal rotating cylindrical heat source. *International Journal of Mechanical Sciences*. 2019; 151: 385–409.
11. Ali MM, Alim MA, Ahmed SS, et al. Magneto hydrodynamic mixed convection flow in a hexagonal enclosure. *Procedia engineering*. 2017;(194):479–486.
12. Kefayati G R. Magnetic field effect on heat and mass transfer of mixed convection of shear-thinning fluids in a lid-driven enclosure with non-uniform boundary conditions. *Journal of the Taiwan Institute of Chemical Engineers*. 2015; 51: 20-33.
13. Akram B, Ullah N, Nadeem S, Eldin SM. Simulations for MHD mixed convection in a partially heated lid-driven chamfered enclosure. *Numeri. Heat. Transf. A Appl*. 2023: 1–21.
14. Maya U M, Alam Md N, Refaie Ali A. Influence of magnetic field on MHD mixed convection in lid-driven cavity with heated wavy bottom surface. *Sci. Rep*. 2023;13 (1):18959.
15. Mliki B, Abbassi MA and Ridha D. CUO–water MHD Mixed Convection Analysis and Entropy Generation Minimisation In Double-Lid-Driven U-Shaped Enclosure with Discrete Heating. *Acta Mechanica et Automatica*. 2023; 17(1): 112-123.
16. Mliki B and Abbassi MA. LBM Analysis of Magneto-Hydrodynamic Mixed Convection of Nanofluid in a Double Lid Driven Heated Incinerator Shaped Cavity with Discrete Heating. *Mathematical Modelling of Fluid Dynamics and Nanofluids*. 2023: 264–282
17. Mliki B and Abbassi MA. Simulation of Magnetic Hybrid Nanofluid (Al₂O₃-Cu/ H₂O) Effect on Natural Convection and Entropy Generation in a Square Enclosure with a Hot Obstacle. *Mathematical Modelling of Fluid Dynamics and Nanofluids*. 2023: 511–525
18. Mliki B, Abbassi MA, Omri A and Belkacem Z. Lattice Boltzmann analysis of MHD natural convection of CuO-water nanofluid in inclined C-shaped enclosures under the effect of nanoparticles Brownian motion. *Powder Technology*. 2017; 308: 70–83.
19. Mliki, B., Abbassi, M. A., Omri, A. Lattice Boltzmann Simulation of Magneto-Hydrodynamics Natural Convection in an L-Shaped Enclosure. *International Journal of Heat And Technology*. 2016; 34 (4).
20. Prosenjit D , Mohammad AH. Predicting MHD mixed convection in a semicircular cavity with hybrid nanofluids using AI. *Heliyon*. 2024; 10:38303.
21. Falah A, Zainab K, Ali K, Raad Z, Hayder I. MHD mixed convection of nanofluid flow Ag- Mgo/water in a channel contain a rotational cylinder. *International Journal of Thermofluids*. 2024; 22: 100713.
22. Mliki B, Abbassi, MA. Analysis of Natural Convection Under the Effect of Nanoparticles Brownian Motion and a Periodic Magnetic Field Utilizing CuO–Water Nanofluid. *J. Nanofluids*. 2024; 13:1123–1133.
23. Ighris Y, Qaffou M, Baliti J, Elguennouni Y, Hssikou M, Thermal management optimization of natural convection in a triangular chamber: Role of heating positions and ternary hybrid Nanofluid. *Physics of Fluids*. 2024; 36: 092002.
24. Ighris Y, BouhouchiY, Baliti J, Hssikou M, Boumezzough A. Numerical study of natural convection in an inclined cavity filled with Al₂O₃/Cu-H₂O nanofluids. *Numerical Heat Transfer, Part A: Applications*. 2024: 1-25. <https://doi.org/10.1080/10407782.2024.2314230>
25. Thilagavathi A, Prasad V R. Thermal Heat Transfer Enhancement Analysis of Magnetic Ternary Hybrid Nanofluid in a Hexagonal Cavity with Square Obstacle. *J. Appl. Comput. Mech*. 2025; 11(1): 239-252.
26. Dipak K M, Nirmalendu B, Nirmal K. M, Rama Subba R G, Chamkha Ali J. Hybrid nanofluid magnetohydrodynamic mixed convection in a novel W-shaped porous system. *International Journal of Numerical Methods for Heat & Fluid*. 2022; 33(10).
27. Dipak K M. Nirmalendu B. Nirmal K M, Rama Subba R G, Chamkha Ali J. Role of surface undulation during mixed bioconvective nanofluid flow in porous media in presence of oxytactic bacteria and magnetic fields. *International Journal of Mechanical Sciences*. 2021; 211: 106778.
28. Mohammed A A, Khaled A F, Qusay H. Al-Salami, Ali I R, Biswas N, Mohamed H, Faris A. Numerical analysis to investigate the effect of a porous block on MHD mixed convection in a split lid-driven cavity with Nanofluid. *International Journal of Thermofluids*. 2024; 22: 100621.
29. Aniket H, Arabdha B, Biswas N, Nirmal K Manna, Dipak K M. MHD nanofluidic mixed convection and entropy generation in a butterfly-shaped cavity. *Sādhanā*. 2024; 49:80.
30. Mliki B, Abbassi MA, Omri A. Lattice Boltzmann Simulation of MHD Double Dispersion Natural Convection in a C-shaped Enclosure in the Presence of a Nanofluid. *Fluid Dynamic and Material Processing*. 2015; 11(1): 87-114.
31. Mliki B, Abbassi MA, Omri A and Belkacem Z. Effects of nanoparticles Brownian motion in a linearly/sinusoidally heated cavity with MHD natural convection in the presence of uniform heat generation/absorption. *Powder Technol*. 2016; 295: 69–83.
32. Maxwell J C. A treatise on electricity and magnetism. Oxford University. Press Cambridge. UK. 1873; 2.
33. Bhatnagar PL, Gross EP and Krook M. A model for collision processes in gases, I: small amplitude processes in charged and neutral one-component systems. *Physical Review*. 1954; 94 (3): 511.
34. Lai FH, Yang YT. Lattice Boltzmann simulation of natural convection heat transfer of Al₂O₃/Water nanofluids in a square enclosure. *Int J of Therm Sci*. 2011; 50: 1930-1941.
35. Ghasemi B, Aminossadati SM, Raisi A. Magnetic field effect on natural convection in a nanofluid-filled square enclosure. *Int J Therm Sci*. 2011; 50:1748–1756.
36. Talebi F, Mahmoudi A H and Shahi M. Numerical study of mixed convection flows in a square lid-driven cavity utilizing Nanofluid. *International Communications in Heat and Mass Transfer*. 2010; 37: 79–90.

Bouchmel Mliki  <https://orcid.org/0000-0002-0200-8060>

Mokhtar Ferhi  <https://orcid.org/0000-0002-6677-3335>

Mohamed A. Abbassi  <https://orcid.org/0000-0002-1915-0944>



This work is licensed under the Creative Commons BY-NC-ND 4.0 license.